Plasmonic analog of electromagnetically induced transparency in multi-nanoresonator-coupled waveguide systems

Hua Lu, Xueming Liu,[*] and Dong Mao

State Key Laboratory of Transient Optics and Photonics, Xi'an Institute of Optics and Precision Mechanics,
Chinese Academy of Sciences, Xi'an 710119, China

We have theoretically and numerically investigated an analog of electromagnetically induced transparency (EIT) in plasmonic systems consisting of multiple cascaded nanodisk resonators, aperture-side-coupled to metal-insulator-metal bus waveguides. A simplified theoretical model is established to study spectral features in the plasmonic waveguide-resonator systems, and the calculated results are in good agreement with finite-difference time-domain simulations. The main dependent factors of EIT-like spectral response, namely, the resonance detuning, intrinsic Drude loss, and especially cavity-cavity separation, are discussed in detail. Similar to multiple EIT in quantum systems, multiple induced-transparency peaks are found in the areas of strong dispersion generated in our plasmonic system. The group indices and quality factors of transparency resonances with high transmission can reach levels of $\sim$35 and $\sim$200, respectively. These results pave a way toward dynamic control of light in the nanoscale domain, which can actualize some new devices for fundamental study and applications of plasmonic nanostructures.

I. INTRODUCTION

Electromagnetically induced transparency (EIT) is a special and counterintuitive phenomenon which occurs in atomic systems due to the quantum destructive interference between the excitation pathways to the atomic upper level [1,2]. The EIT effect has promising applications in nonlinear optical processes, ultrafast switching, and optical data storage owing to the strong dispersion in the transparency windows [3,4]. However, on-chip applications of the atomic EIT are severely limited by the rigorous conditions such as low-temperature environments and stable gas lasers [4]. Recently, theoretical analysis and experimental observations demonstrate that a novel phenomenon analogous to EIT can occur in the coupled optical resonator systems due to the coherent interference of coupled resonators, which is known as coupled-resonator induced transparency (CRIT) [5–10]. The CRIT effect in coupled resonator systems is remarkably analogous to the conventional EIT in atomic systems [10]. For example, Xu *et al.* first reported the experimental observation of the EIT-like spectrum in integrated optical resonator systems consisting of coupled silicon ring resonators [6]. Yang *et al.* reported the first observation of the all-optical EIT-like spectral response in multiple coupled photonic crystal (PC) cavities [7]. The EIT-like spectral response was also found in the coupled whispering-gallery microresonators [8], with observations of slow-light effect [9]. The on-chip footprint and field confinement of conventional photonic devices are physically limited by the fundamental laws of classical diffraction [11].

Nowadays, novel techniques for controlling light on a small scale increasingly promote the development of optical physics [3]. Electromagnetic waves trapped on metal-dielectric interfaces and coupled to propagating free-electron oscillations in the metals are known as surface plasmon polaritons (SPPs), which are regarded as one of the most promising technologies for the minimization of on-chip integrated devices owing to their capabilities to overcome the classical diffraction limit and manipulate light in the nanoscale domain [11–14]. A large amount of plasmonic components with special functions are proposed and demonstrated both numerically and experimentally in the metallic nanostructures [15–21]. Recently, the plasmonic analog of EIT has been investigated intensively in metamaterials [22]. Plasmonic waveguides such as the metal-insulator-metal (MIM) structure are attracting much attention due to their particularly strong confinement of light [11,23,24], which can be well employed to realize truly nanoscale photonic functionality [11]. Spectral features such as the EIT-like performance in plasmonic waveguide-resonator systems are also very important for dynamic control and manipulation of light in the nanostructures [25,26].

The EIT-like spectral response performed in waveguide-resonator systems exhibits two physical pictures: a radiative (coupled to waveguide) resonator coupled with a subradiant (not coupled to waveguide) resonator [5,8,9,26] or two detuned resonators coupled to a bus waveguide [4,6,7,25]. The latter scheme is essential for the observation of EIT-like and slow-light effects [4]. As an important phenomenon, a multi-EIT-like spectral response was realized in PC resonator systems [7]. Can similar behavior be performed in plasmonic waveguide-resonator systems? Which factors would determine the EIT-like response? The current paper answers these questions. In this paper, we not only study numerically the multiple EIT-like and slow-light effects in a type of plasmonic waveguide-resonator systems, but also obtain consistent results by means of the derived theoretical model. Theoretical and simulation results reveal that the EIT-like response mainly depends on the resonance detuning, intrinsic Drude loss, and cavity-cavity separation. It is found that transparency-resonance peaks

---

*Corresponding author (X. Liu). Tel.: +862988881560; fax: +862988887603; electronic mail: liuxueming72@yahoo.com and liuxm@opt.ac.cn

possess a high quality factor, group indices, and transmission efficiencies.

II. PLASMONIC SYSTEMS AND THEORETICAL MODEL

A cross-section schematic diagram of our plasmonic systems is shown in Fig. 1. It consists of a MIM bus waveguide with multiple asymmetrically aperture-side-coupled dielectric nanodisk resonators. When a transverse-magnetic (TM) light is injected and coupled into the bus waveguide, SPP wave forms on the metallic interfaces and is confined in the waveguide. As the SPP wave passes through the coupled aperture, the energy can be coupled into the nanodisk resonator through the dielectric aperture. A single disk transmission spectrum exhibits a dip at the resonance wavelength due to the destructive interference between the incident wave and escaped power from the resonator. For the multi-resonator-coupled waveguide systems in Fig. 1, the dynamic transmission features can be investigated by a temporal coupled-mode theory [27]. To simplify the theoretical model, the light propagation and coupling losses are not considered. For the harmonic time dependence of $e^{-j\omega t}$, the temporal normalized mode amplitudes a_i of the ith cavity ($i = 1, 2, \ldots, N$) can be described as

$$\frac{da_i}{dt} = (-j\omega_i - \kappa_{o,i} - \kappa_{e,i})a_i + e^{j\theta_i}\sqrt{\kappa_{e,i}}S_{+,\text{in}}^{(i)}$$
$$+ e^{j\theta_i}\sqrt{\kappa_{e,i}}S_{-,\text{in}}^{(i)}, \tag{1}$$

where ω_i represents the resonance frequency of the ith cavity, $\kappa_{o,i}$ is the decay rate of the field due to internal loss in the ith cavity, and $\kappa_{e,i}$ is the decay rate due to the energy escape into the waveguide. The decay rates satisfy the relationships $\kappa_{o,i} = \omega_i/(2Q_{o,i})$, $\kappa_{e,i} = \omega_i/(2Q_{e,i})$. Here, $Q_{o,i}$ and $Q_{e,i}$ stand for the intrinsic and coupling quality factors of the ith cavity, respectively. θ_i is the phase of coupling coefficient. The dielectric cavities and apertures possess mirror symmetry with respect to the reference planes. The amplitudes of the incoming
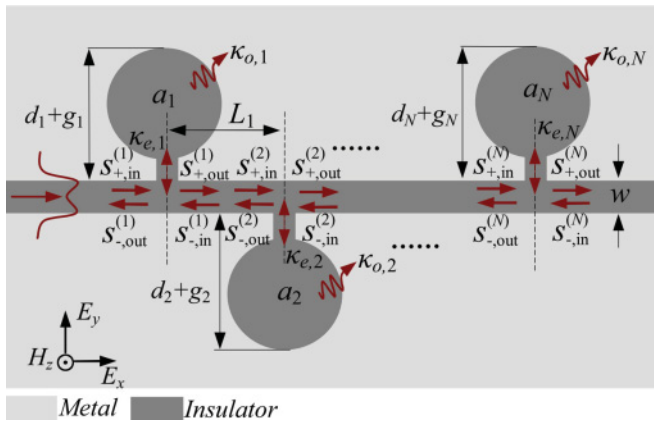

FIG. 1. (Color online) Schematic diagram of plasmonic multi-nanoresonator-coupled waveguide systems. d_i and g_i represent the diameter and aperture-coupled length of cavity i ($i = 1, 2, \ldots, N$), respectively. w and L_i are the width of the MIM bus waveguide and the separation between cavities i and $i + 1$, respectively. The dashed lines are reference planes in the middle of nanodisk cavities. The other parameters are present in the text.

and outgoing waves in the bus waveguide are depicted by $S_{p,\text{in}}^{(i)}$, and $S_{p,\text{out}}^{(i)}$ ($i = 1, 2, \ldots, N$). The subscript p $= \pm$ represent two propagating directions of waveguide modes, as shown in Fig. 1. From energy conservation, the outgoing waves of the ith cavity can be written as

$$S_{-,\text{out}}^{(i)} = S_{-,\text{in}}^{(i)} - e^{-j\theta_i}\sqrt{\kappa_{e,i}}a_i, \tag{2a}$$

$$S_{+,\text{out}}^{(i)} = S_{+,\text{in}}^{(i)} - e^{-j\theta_i}\sqrt{\kappa_{e,i}}a_i. \tag{2b}$$

In the linear system, since the input frequency is ω, the field everywhere oscillates as $e^{-j\omega t}$, and $da_i/dt = -j\omega a_i$. The relation between incoming and outgoing waves of the ith cavity can be expressed as

$$S_{-,\text{in}}^{(i)} = \frac{\kappa_{e,i}}{j(\omega_i - \omega) + \kappa_{o,i}}S_{+,\text{in}}^{(i)}$$
$$+ \frac{j(\omega_i - \omega) + \kappa_{o,i} + \kappa_{e,i}}{j(\omega_i - \omega) + \kappa_{o,i}}S_{-,\text{out}}^{(i)}, \tag{3a}$$

$$S_{+,\text{out}}^{(i)} = \frac{j(\omega_i - \omega) + \kappa_{o,i} - \kappa_{e,i}}{j(\omega_i - \omega) + \kappa_{o,i}}S_{+,\text{in}}^{(i)}$$
$$- \frac{\kappa_{e,i}}{j(\omega_i - \omega) + \kappa_{o,i}}S_{-,\text{out}}^{(i)}. \tag{3b}$$

When the light is only inputted from the left port ($S_{-,\text{in}}^{(i)} = 0$), the transmission and reflection coefficients of the single-resonator-coupled waveguide system are derived as

$$t_i(\omega) = \frac{j(\omega_i - \omega) + \kappa_{o,i}}{j(\omega_i - \omega) + \kappa_{o,i} + \kappa_{e,i}}, \tag{4a}$$

$$r_i(\omega) = -\frac{\kappa_{e,i}}{j(\omega_i - \omega) + \kappa_{o,i} + \kappa_{e,i}}. \tag{4b}$$

Consequently, incoming and outgoing waves of the ith cavity in multi-resonator-coupled waveguide systems satisfy the following transfer equation:

$$\begin{bmatrix} S_{-,\text{in}}^{(i)} \\ S_{+,\text{out}}^{(i)} \end{bmatrix} = \begin{pmatrix} -\frac{r_i(\omega)}{t_i(\omega)} & \frac{1}{t_i(\omega)} \\ 1 + \frac{r_i(\omega)}{t_i(\omega)} & \frac{r_i(\omega)}{t_i(\omega)} \end{pmatrix} \begin{bmatrix} S_{+,\text{in}}^{(i)} \\ S_{-,\text{out}}^{(i)} \end{bmatrix}. \tag{5}$$

From Eq. (5), the side-coupled cavities can be regarded as frequency-dependent lossy mirrors [$r_i^2(\omega) + t_i^2(\omega) < 1$]. The propagation waves in the bus waveguide should satisfy the relationship in the steady state:

$$S_{-,\text{in}}^{(i)} = S_{-,\text{out}}^{(i+1)}e^{j\varphi_i}, \; S_{+,\text{in}}^{(i+1)} = S_{+,\text{out}}^{(i)}e^{j\varphi_i}. \tag{6}$$

Here φ_i ($i = 1, 2, \ldots, N - 1$) represents the phase difference between the ith and $(i + 1)$th cavities. The matrices are defined as

$$V_i = \begin{pmatrix} -\frac{r_i(\omega)}{t_i(\omega)} & \frac{1}{t_i(\omega)} \\ 1 + \frac{r_i(\omega)}{t_i(\omega)} & \frac{r_i(\omega)}{t_i(\omega)} \end{pmatrix}, \quad M_i = \begin{pmatrix} 0 & e^{j\varphi_i} \\ e^{-j\varphi_i} & 0 \end{pmatrix}. \tag{7}$$

Thus, incident and output waves in the entire system show a transfer characteristic and can be described as

$$\begin{bmatrix} S_{-,\text{in}}^{(N)} \\ S_{+,\text{out}}^{(N)} \end{bmatrix} = V_N M_{N-1} V_{N-1} M_{N-2} \cdots V_2 M_1 V_1 \begin{bmatrix} S_{+,\text{in}}^{(1)} \\ S_{-,\text{out}}^{(1)} \end{bmatrix}. \tag{8}$$

We assume

$$H = V_N M_{N-1} V_{N-1} M_{N-2} \cdots V_2 M_1 V_1 = \begin{pmatrix} H_{11} & H_{12} \\ H_{21} & H_{22} \end{pmatrix}. \tag{9}$$

When the incident light is launched only from the left waveguide ($S_{-,\text{in}}^{(N)} = 0$), the output transmission efficiency in the entire waveguide-resonator system can be derived as

$$T = \left| \frac{S_{+,\text{out}}^{(N)}}{S_{+,\text{in}}^{(1)}} \right|^2 = \left| \frac{H_{21}H_{12} - H_{22}H_{11}}{H_{12}} \right|^2. \quad (10)$$

III. EIT-LIKE RESPONSE IN DUAL-RESONATOR-COUPLED SYSTEMS

A. Waveguide dispersion and quality factors

The cavity-cavity phase difference φ_i in Eq. (6) for the plasmonic waveguide is expressed as

$$\varphi_i = \text{Re}(\beta_{spp})L_i = \frac{\omega \text{Re}(n_{\text{eff}})L_i}{c}, \quad (11)$$

where L_i ($i = 1,2,\ldots,N-1$) is the optical path difference between the ith and $(i+1)$th cavities. β_{spp} is the complex propagation constant of the SPP wave, c is the light velocity in vacuum, and n_{eff} is the effective refractive index which can be obtained by solving the dispersion equation [15],

$$\varepsilon_m \sqrt{n_{\text{eff}}^2 - \varepsilon_d} \tanh\left(\frac{w\pi\sqrt{n_{\text{eff}}^2 - \varepsilon_d}}{\lambda} \right) + \varepsilon_d\sqrt{n_{\text{eff}}^2 - \varepsilon_m} = 0, \quad (12)$$

where ε_m and ε_d stand for the dielectric constant of metal cladding and dielectric waveguide with a width of w. In the plasmonic systems, the metal cladding is assumed as silver, whose frequency-dependent complex relative permittivity can be described by the well-known Drude model of $\varepsilon_m(\omega) = \varepsilon_\infty - \omega_p^2/(\omega^2 + j\omega\gamma)$ [15,25]. Here, ε_∞ is the dielectric constant at the infinite frequency, and γ and ω_p stand for the electron collision and bulk plasma frequencies, respectively. These parameters for silver can be set as $\varepsilon_\infty = 3.7$, $\omega_p = 9.1$ eV, and $\gamma = 0.018$ eV [15]. The width of the bus waveguide is assumed as 50 nm (i.e., $w = 50$ nm). The insulator in the waveguide-resonator systems is set as air ($\varepsilon_d = 1$). The real part of the refractive index obtained by solving Eq. (12) is shown in Fig. 2(a).

The multi-resonator-coupled waveguide configurations are the generalization of the dual-resonator-coupled system. Therefore, the fundamental features of the dual-resonator-coupled system are very important for investigating the EIT-like effect in plasmonic waveguide-resonator systems. For dual-resonator-coupled waveguide systems ($N = 2$), the output transmission efficiency can be derived as

$$T = \left| \frac{S_{+,\text{out}}^{(2)}}{S_{+,\text{in}}^{(1)}} \right|^2 = \left| \frac{t_1 t_2}{1 - r_1 r_2 e^{j2\varphi_1}} \right|^2. \quad (13)$$

The above equation is a typical form of the transmission spectrum of a Fabry-Perot resonator with two frequency-dependent mirrors [4]. Therefore, the physical mechanism of the spectral response in the plasmonic waveguide can be contributed to the Fabry-Perot oscillation. $r_{1,2}$ and $t_{1,2}$ are the
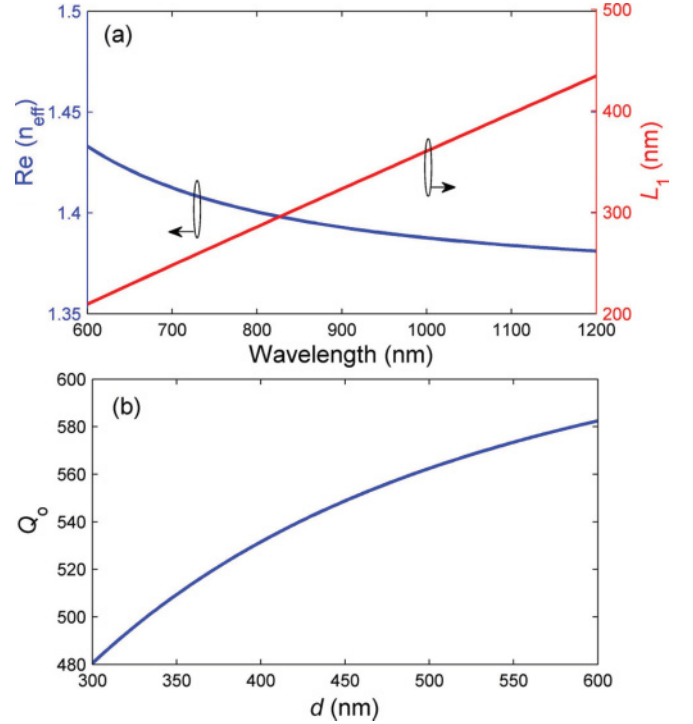

FIG. 2. (Color online) (a) Real part of the effective refractive index in the MIM bus waveguide with $w = 50$ nm. The approximately optimal separation L_1 corresponds to the cavity-cavity phase of π for the central wavelength. (b) Intrinsic quality factor (Q_o) versus the diameter of the nanodisk resonator.

frequency-dependent reflection and transmission coefficients of mirrors 1 and 2, which can be achieved from Eq. (4).

The quality factors $Q_{o,1}$, $Q_{o,2}$, $Q_{e,1}$, and $Q_{e,2}$ should be obtained for the theoretical investigation of the transmission response in the dual-resonator-coupled system. Here, the intrinsic quality factor Q_o of the dielectric cavity can be estimated from the following equations [28]:

$$\frac{\sqrt{\varepsilon_m}J_n'(k\sqrt{\varepsilon_d}d/2)}{J_n(k\sqrt{\varepsilon_d}d/2)} - \frac{\sqrt{\varepsilon_d}H_n^{(1)'}(k\sqrt{\varepsilon_m}d/2)}{H_n^{(1)}(k\sqrt{\varepsilon_m}d/2)} = 0, \quad (14)$$

$$Q_o = -\frac{\text{Re}(k)}{2\text{Im}(k)}, \quad (14b)$$

where d is the diameter of the nanocavity. k is the wave number in vacuum and includes a relatively small negative imaginary part for a given n, where the negative imaginary part presents the loss [28]. J_n and J_n' are Bessel function of the first kind with the order n and its derivative, $H_n^{(1)}$ and $H_n^{(1)'}$ are the first kind Hankel function with the order n and its derivative, respectively. The fundamental mode is considered in the frequency range, which corresponds to the first-order ($n = 1$) Bessel and Hankel functions. From Eq. (14), Q_o as a function of the diameter of the nanodisk cavity is shown in Fig. 2(b). The total quality factor (Q_t) of the side-coupled cavity can be estimated from $Q_t = \lambda_0/\Delta\lambda$, where λ_0 and $\Delta\lambda$ are the peak wavelength and the FWHM of the reflection spectrum, respectively. Under the condition of $Q_o \gg Q_e$, the quality factor (Q_e) owing to the power escape into the waveguide can be obtained from the equation $Q_e = Q_o Q_t/(Q_o - Q_t)$.
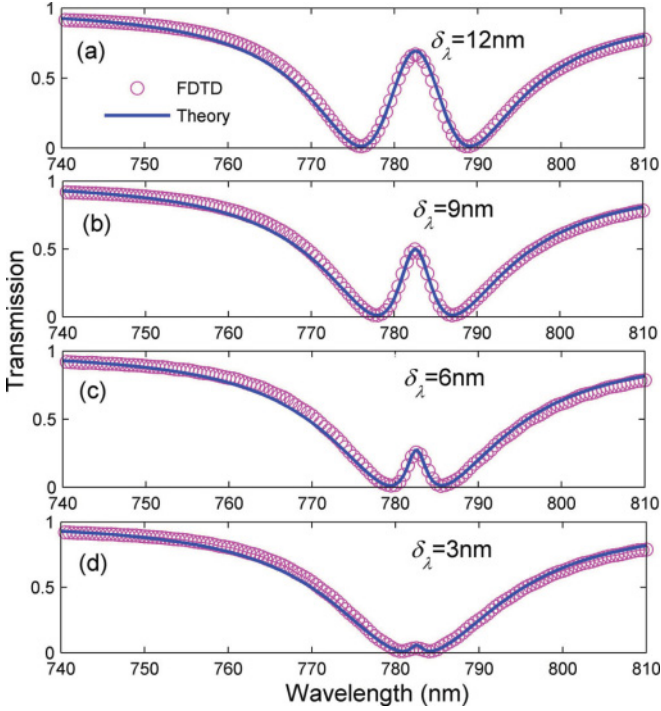
FIG. 3. (Color online) Transmission spectra with various wavelength detuning σ_λ in the plasmonic dual-nanoresonator-coupled waveguide with $L_1 = 280$ nm. The circles are the simulation results and the solid curves are the theoretical calculations. The diameters (d_1 and d_2) of cavities 1 and 2 are set as 391 and 399 nm (a), 392 and 398 nm (b), 393 and 397 nm (c), and 394 and 396 nm (d).

In our structure, the coupling distances g_1 and g_2 are fixed at 100 nm. The widths of coupling aperture are 20 nm. The diameter of cavity 1 (2) is set from 391 (399) nm to 394 (396) nm at an interval of 1(−1) nm. As depicted in Fig. 2(b), Q_o is about 530 for the above diameters. Using the finite-difference time-domain (FDTD) method [29], Q_t is calculated at about 60 with selected physical parameters. Thus, Q_e is about 67.7 for the side-coupled resonators.

B. Dependence of the transparency peak on resonance detuning and intrinsic loss

As shown in Fig. 3, the transmission spectra exhibit typical EIT line shapes, namely, a narrow transparency peak in the center of a broader transmission dip [6]. The resonance wavelengths λ_1 and λ_2 for cavities 1 and 2 are controlled by adjusting the diameters. The wavelength difference $\sigma_\lambda = |\lambda_1 - \lambda_2|$ is termed detuning [25]. From the Fabry-Perot theoretical model, the transmission will be enhanced if the Fabry-Perot resonant condition is satisfied. The pronounced EIT-like transparency peak appears at $(\omega_1 + \omega_2)/2$ when the cavity-cavity phase φ_1 satisfies $m\pi$ ($m = 1, 2, \ldots$) [7]. Because $4\pi c/(\omega_1 + \omega_2)$ approaches the central wavelength $(\lambda_1 + \lambda_2)/2$ here, the transparency peak nearly locates at the central wavelength [25]. As shown in Fig. 3, transparency-resonance peaks locate at the central wavelength of 782.5 nm. From Eq. (11), φ_1 equals π at $\lambda_{12} = (\lambda_1 + \lambda_2)/2$ when $L_1 = \lambda_{12}/[2\mathrm{Re}(n_{\mathrm{eff}})]$. The optimal cavity-cavity separation L_1 plotted in Fig. 2(a) is about 280 nm at 782.5 nm, which
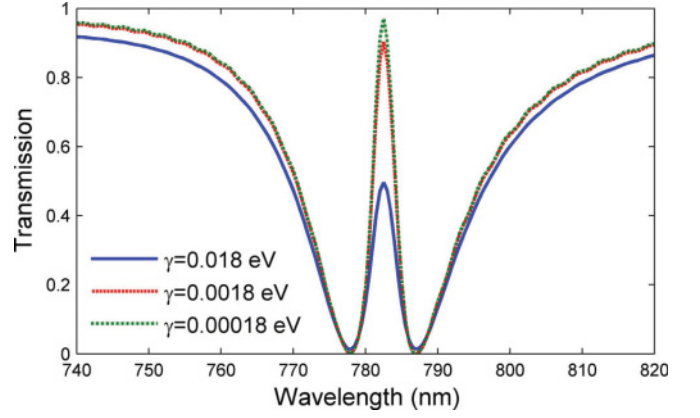

FIG. 4. (Color online) Transmission spectra with different electron collision frequencies γ which represents the intrinsic Drude loss of silver. Here $L_1 = 280$ nm, and the diameters of cavities 1 and 2 are 392 and 398 nm, respectively.

agrees well with the parameter setting. The spectral responses in the systems are investigated by the FDTD simulations and theoretical model. Figure 3 reveals that the transparency peaks possess symmetrical profiles. A smaller detuning induces a narrower spectral bandwidth (higher quality factor) but a reducing peak transmission. Therefore, there exists a tradeoff between the peak transmission and quality factor [4]. The cavity detuning offers a convenient scheme to control the quality factor of the transparency resonance. The theoretical results are in good agreement with FDTD simulations. In the FDTD scheme, perfectly matched absorbing boundary conditions are employed to absorb outgoing waves from the computation domain [29]. The spatial and temporal steps are set as $\Delta x = \Delta y = 2$ nm and $\Delta t = \Delta x/2c$, respectively.

Successively, the EIT-like effect is investigated in the plasmonic systems with different metal (intrinsic Drude) loss. As shown in Fig. 4, the transparency-resonance transmission and quality factor increases with the decrease of the electron collision frequency of the metal (i.e., damping factor of the silver). The result illustrates that the EIT-like spectral response is limited by the intrinsic Drude loss of metal material. Thus, a gain material could be inserted into the waveguide system to compensate the Drude loss [30], which thereby achieves a more obvious EIT-like effect and higher quality factor.

C. Influence of cavity-cavity separation on the transparency peak

The round-trip phase of the Fabry-Perot cavity is controlled by the optical path difference between the two mirrors. The transmission properties will be changed by adjusting the cavity-cavity separation L_1. Figure 5 reveals the transmission spectra at the various values of L_1, which are calculated by the FDTD method and dynamic equations. Here, the diameters are set as $d_1 = 392$ nm and $d_2 = 398$ nm. It is found that the resulting transparency line is very low, as L_1 is around 140 nm, where the transmission waves through two mirrors generate the destructive interference around the transparency wavelength. The transmission spectrum possesses a narrow, symmetric peak in the middle of the transparency window when
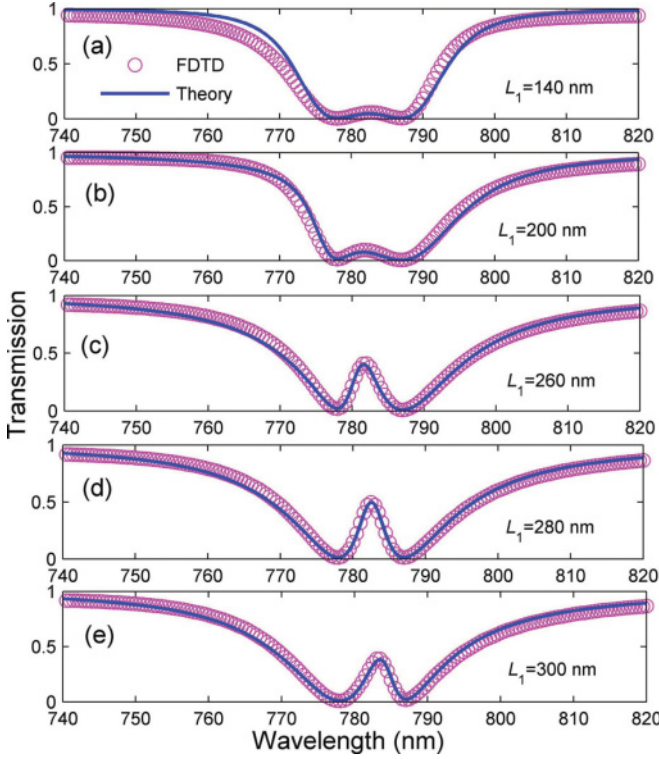
FIG. 5. (Color online) Simulation (circles) and theoretical (solid curve) transmission spectra with the different cavity-cavity separation L_1. The diameters of cavities 1 and 2 are 392 and 398 nm, respectively.

FIG. 6. (Color online) (a) Evolution of transmission spectrum with cavity-cavity separation L_1. (b) M and P at different L_1. M represents the maximum possible output transmission. P includes the phase term of the Fabry-Perot cavity and controls the transmission spectral features.

$L_1 = 280$ nm, which derives from the constructive interference of transmission waves at the central wavelength. Moreover, the transparency-resonance peak becomes asymmetric and blue-(red-) tilted when $L_1 = 260$ (300) nm, respectively. To further clarify the spectral features, the evolution of the transmission spectrum with separation L_1 is depicted in Fig. 6(a). We find that the transparency peaks exhibit obvious and redshift around $L_1 = 280$ nm. The optical behavior can be distinctly explained by the Fabry-Perot model. The dynamical equation in Eq. (13) can be also expressed in the following form:

$$T = \left(\frac{|t_1 t_2|}{1 - |r_1 r_2|}\right)^2 \frac{1}{1 + 4\left(\frac{\sqrt{|r_1 r_2|}}{1 - |r_1 r_2|}\right)^2 \sin^2 \theta}. \quad (15)$$

Here, $\theta = Arg[r_1 r_2 \exp(j2\varphi_1)]/2$ is one-half of the round-trip phase in the Fabry-Perot cavity. The transmission can be written as $T = MP$, where $M = [|t_1 t_2|/(1 - |r_1 r_2|)]^2$ and $P = 1/\{1 + 4[|r_1 r_2|/(1 - |r_1 r_2|)^2] \sin^2 \theta\}$. M stands for the maximum possible output transmission through the plasmonic waveguide. The term P containing the phase information of the Fabry-Perot resonator will influence the transmission response as the cavity-cavity separation L_1 changes. Figure 6(b) describes the results of M and P with the different L_1. It is found that M possesses an EIT-like line shape. P is symmetric and has a minimum at the transparency-resonance wavelength when $L_1 = 140$ nm. Thus, P suppresses the generation of the EIT-like peak, as shown in Fig. 5(a). Meanwhile, P exhibits symmetric and has maximum at the transparency-peak wavelength when $L_1 = 280$ nm, which gives rise to a pronounced and symmetric EIT-like spectral response. When $L_1 = 260$ nm (300 nm), P becomes asymmetric and its
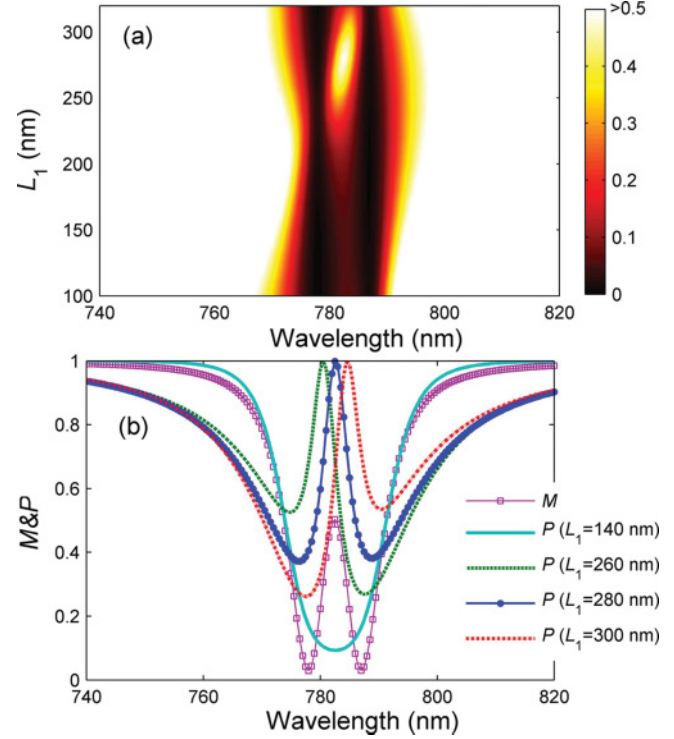
maximum shifts to the left (right) side of the peak wavelength of M. This performance induces the asymmetric and blue (red)-tilted EIT-like peak, as shown in Figs. 5(c) and 5(e). The peak location of P corresponds to the resonance wavelength of the Fabry-Perot cavity. Essentially, the movement of the EIT-like transmission peak is contributed to the redshift of the Fabry-Perot resonance wavelength with the increase of cavity-cavity separation at around 280 nm.

D. Slow-light effect

Similar to the EIT effect in the atomic system, our plasmonic systems also support slow group velocities. The slow-light effect can be described by the group index n_g, which is expressed as

$$n_g = \frac{c}{v_g} = \frac{c}{D}\tau_g = \frac{c}{D} \cdot \frac{d\psi(\omega)}{d\omega}. \quad (16)$$

Here v_g stands for the group velocity in the plasmonic waveguide systems. τ_g and $\psi(\omega)$ are the optical delay time and transmission phase shift, respectively. D is the length of the plasmonic system. The slow-light behavior is numerically investigated in the waveguide-resonator system with $d_1 = 392$ nm, $d_2 = 398$ nm, $L_1 = 280$ nm, and $D = 1 \mu$m. Figure 7(a) illustrates that the phase slope is negative and steepest at the location of the EIT-like peak. This ultracompact configuration exhibits the large optical delay in the transparency window, with a maximum delay time of about 0.12 ps at the transparency-peak wavelength as shown in Fig. 7(b). The
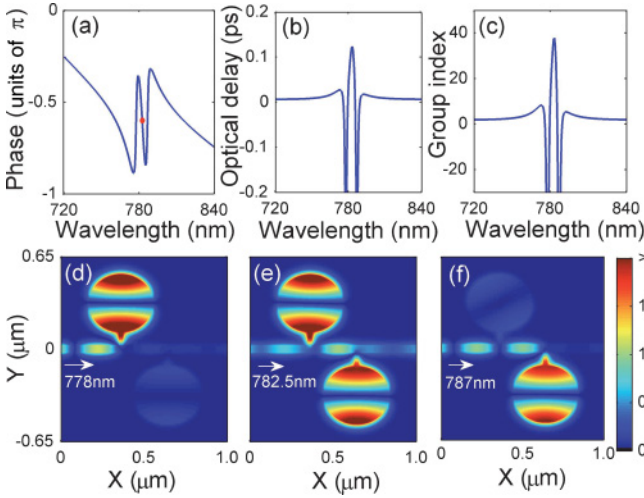
FIG. 7. (Color online) (a) Transmission phase shift, (b) optical delay line, and (c) group indices in the plasmonic system with $d_1 = 392$ nm, $d_2 = 398$ nm, and $L_1 = 280$ nm. The dot shows the location of the EIT-like peak. (d)–(f) Average field distributions of $|H_Z|$ at the resonance wavelengths of cavities 1 (d) and 2 (f) as well as transparency-resonance wavelength (e). The input direction is marked by the white arrow. See Supplemental Material at [http://link.aps.org/supplemental/10.1103/PhysRevA.85.053803] for the multimedia file corresponding to the simulation of (e) [31].

negative group delay corresponding to the fast light is observed at the two sides of the transparency window [9]. The group indices are depicted in Fig. 7(c). High group indices around the transparency peak result from the strong dispersion in the transparency window. The maximum group index is over 35 at the transparency-peak wavelength. The corresponding quality factor of the transparency-peak resonance reaches the level of ∼200, as shown in Fig. 5(d).

In addition, the field distributions at the individual resonance and transparency-resonance wavelengths are plotted in Figs. 7(d)–7(f). With the physical parameters in Fig. 7(a), the resonance wavelengths of cavities 1 and 2 are located at 778 and 787 nm, respectively. When the incident wavelength is 778 or 787 nm, the local resonance is excited in the individual side-coupled cavity and the incident light is reflected, as depicted in Figs. 7(d) and 7(f). For the transparency-resonance wavelength, the two partially resonant cavities form a Fabry-Perot oscillation in the bus waveguide, and the incident light can pass through the waveguide, as shown in Fig. 7(e) and [31]. This performance is counterintuitive for side-coupled resonator systems. The field distributions are consistent with the transmission spectrum in Fig. 3(b).

IV. MULTIPEAK EIT-LIKE RESPONSE

Finally, a plasmonic triple-resonator-coupled waveguide system is designed as an example to investigate the multipeak EIT-like transmission response and multiarea slow-light effect. The diameters of cavities 1, 2, and 3 are set as 392, 398, and 404 nm, respectively. The cavity-cavity separations L_1 and L_2 are 280 nm, and D is 1.2 μm. The other physical parameters are the same as the sample in Sec. III. According to the results in Sec. III A, the intrinsic quality factor (Q_o) and coupling quality
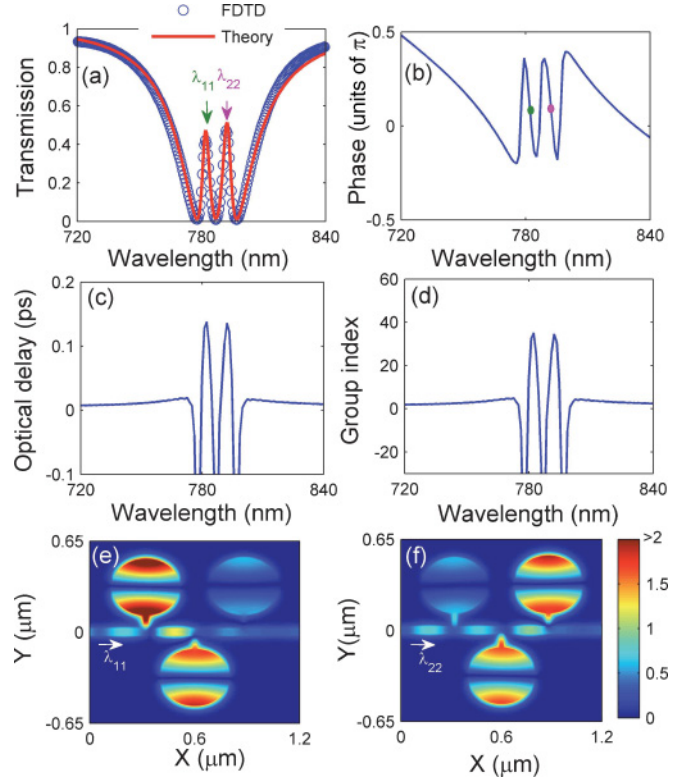

FIG. 8. (Color online) (a) Simulation (circles) and theoretical (solid curve) transmission spectrum in the triple-nanoresonator-coupled waveguide system with $d_1 = 392$ nm, $d_2 = 398$ nm, $d_3 = 404$ nm, $L_1 = L_2 = 280$ nm, and $g_1 = g_2 = 100$ nm. (b) Corresponding transmission phase shift, (c) optical delay line, and (d) group indices in the transparency windows. The dots in (b) show the locations of the two EIT-like peaks. Average field distributions of $|H_Z|$ at the two transparency-resonance wavelengths: (e) $\lambda_{11} = 782.5$ nm and (f) $\lambda_{22} = 792$ nm.

factor (Q_e) of these side-coupled cavities can also be estimated as 530 and 67.7, respectively. As shown in Fig. 8(a), the transmission spectrum calculated by the theoretical model is in accordance with the FDTD simulation. There are two EIT-like peaks at the wavelengths λ_{11} (782.5 nm) and λ_{22} (792 nm) in the transmission spectrum. Transmission phase shift, optical delay line, and group indices are respectively depicted in Figs. 8(b)–8(d). The results show that two slow-light areas are realized in the transparency windows. The maximal group indices are about 35 at the two transparency-peak wavelengths. The quality factors of transparency resonances retain the level of ∼200. Figures 8(e) and 8(f) show the average magnetic field distributions at the transparency-peak wavelengths. The generation of the first EIT-like peak is contributed to the Fabry-Perot resonance building in the bus waveguide between cavities 1 and 2. Another EIT-like peak occurs due to the satisfaction of the Fabry-Perot resonant condition in the bus waveguide between cavities 2 and 3. The incident lights can pass through the plasmonic waveguide system, which is consistent with the result in Fig. 8(a). This sample is only an example of multi-resonator-coupled waveguide systems. $N-1$ areas of EIT-like transparency windows can be realized in the plasmonic waveguide with N aperture-side-coupled resonators.

V. CONCLUSIONS

The EIT-like spectral response has been investigated theoretically and numerically in plasmonic systems which consist of multiple cascaded nanodisk resonators aperture-side-coupled to MIM bus waveguides. The simplified theoretical model has been derived from the temporal coupled-mode theory, which shows that plasmonic multi-resonator systems can be regarded as arrays of wavelength-filtering lossy mirrors. For the two-resonator system, the theoretical and simulation results have illustrated that the decrease of resonance detuning between the side-coupled cavities gives rise to narrower EIT-like spectral responses but at the expense of dropping peak transmission. The decrease of the intrinsic Drude loss induces a higher transparency-resonance quality factor and peak transmission. The transmission spectrum exhibits the symmetrical EIT-like line shape when the cavity-cavity round-trip phase satisfies the condition of Fabry-Perot resonance. With the increase of cavity-cavity separation at around the optimum length, the transparency peak possesses a redshift which can be accurately analyzed by the Fabry-Perot theoretical model. Similar to the multiple EIT in atomic systems, multiple EIT-like transparency windows have been found in the plasmonic waveguide-resonator systems. Our ultracompact configurations can realize group indices of ∼35 and quality factors of about 200, as well as retain high peak transmission. They can find important potential applications in highly integrated optical circuits and networks, especially for wavelength-selective, ultrafast switching, light storage and nonlinear devices.

[1] K. J. Boller, A. Imamoglu, and S. E. Harris, Phys. Rev. Lett. **66**, 2593 (1991).

[2] M. Fleischhauer, A. Imamoglu, and J. P. Marangos, Rev. Mod. Phys. **77**, 633 (2005).

[3] R. W. Boyd and D. J. Gauthier, Nature (London) **441**, 701 (2006).

[4] R. D. Kekatpure, E. S. Barnard, W. Cai, and M. L. Brongersma, Phys. Rev. Lett. **104**, 243902 (2010).

[5] D. D. Smith, H. Chang, K. A. Fuller, A. T. Rosenberger, and R. W. Boyd, Phys. Rev. A **69**, 063804 (2004).

[6] Q. Xu, S. Sandhu, M. L. Povinelli, J. Shakya, S. Fan, and M. Lipson, Phys. Rev. Lett. **96**, 123901 (2006).

[7] X. Yang, M. Yu, D. L. Kwong, and C. W. Wong, Phys. Rev. Lett. **102**, 173902 (2009).

[8] A. Naweed, G. Farca, S. I. Shopova, and A. T. Rosenberger, Phys. Rev. A **71**, 043804 (2005).

[9] K. Totsuka, N. Kobayashi, and M. Tomita, Phys. Rev. Lett. **98**, 213904 (2007).

[10] Y. F. Xiao, X. B. Zou, W. Jiang, Y. L. Chen, and G. C. Guo, Phys. Rev. A **75**, 063833 (2007).

[11] R. Zia, J. A. Schuller, A. Chandran, and M. L. Brongersma, Mater. Today **9**, 20 (2006).

[12] W. L. Barnes, A. Dereux, and T. W. Ebbesen, Nature (London) **424**, 824 (2003).

[13] S. I. Bozhevolnyi, V. Volkov, E. Devaux, J. Laluet, and T. Ebbesen, Nature (London) **440**, 508 (2006).

[14] Q. Q. Gan, Y. Gao, Q. Wang, L. Zhu, and F. Bartoli, Phys. Rev. B **81**, 085443 (2010).

[15] J. Park, H. Kim, and B. Lee, Opt. Express **16**, 413 (2008); Z. Han, E. Forsberg, and S. He, IEEE Photonics Technol. Lett. **19**, 91 (2007); P. B. Johnson and R. W. Christy, Phys. Rev. B **6**, 4370 (1972).

[16] Q. Gan, Y. J. Ding, and F. J. Bartoli, Phys. Rev. Lett. **102**, 056801 (2009); Q. Gan, Z. Fu, Y. J. Ding, and F. J. Bartoli, *ibid.* **100**, 256803 (2008).

[17] G. A. Wurtz, R. Pollard, and A. V. Zayats, Phys. Rev. Lett. **97**, 057402 (2006); C. Min, P. Wang, C. Chen, Y. Deng, Y. Lu, H. Ming, T. Ning, Y. Zhou, and G. Yang, Opt. Lett. **33**, 869 (2008); H. Lu, X. Liu, L. Wang, Y. Gong, and D. Mao, Opt. Express **19**, 2910 (2011).

[18] G. Veronis and S. Fan, Appl. Phys. Lett. **87**, 131102 (2005); Z. Han, A. Elezzabi, and V. Van, *ibid.* **96**, 131106 (2010); H. Lu, X. M. Liu, D. Mao, L. Wang, and Y. Gong, Opt. Express **18**, 17922 (2010).

[19] T. Nikolajsen, K. Leosson, and S. I. Bozhevolnyi, Appl. Phys. Lett. **85**, 5833 (2004).

[20] I. Leon and P. Berini, Nat. Photonics **4**, 382 (2010).

[21] A. Drezet, D. Koller, A. Hohenau, A. Leitner, F. Aussenegg, and J. Krenn, Nano Lett. **7**, 1697 (2007); H. Lu, X. Liu, Y. Gong, D. Mao, and L. Wang, Opt. Express **19**, 12885 (2011).

[22] S. Zhang, D. A. Genov, Y. Wang, M. Liu, and X. Zhang, Phys. Rev. Lett. **101**, 047401 (2008); N. Liu, Nat. Mater. **8**, 758 (2009).

[23] P. Neutens, P. Van Dorpe, I. De Vlaminck, L. Lagae, and G. Borghs, Nat. Photonics **3**, 283 (2009).

[24] J. A. Dionne, L. A. Sweatlock, H. A. Atwater, and A. Polman, Phys. Rev. B **73**, 035407 (2006).

[25] Z. Han and S. Bozhevolnyi, Opt. Express **19**, 3251 (2011).

[26] H. Lu, X. Liu, D. Mao, Y. Gong, and G. Wang, Opt. Lett. **36**, 3233 (2011).

[27] H. A. Haus, *Waves and Fields in Optoelectronics*, Chap. 7 (Prentice-Hall, Englewood Cliffs, NJ, 1984); C. Manolatou, M. Khan, S. Fan, P. Villeneuve, H. A. Haus, and J. D. Joannopoulos, IEEE J. Quantum Electron. **35**, 1322 (1999).

[28] I. Chremmos, J. Opt. Soc. Am. A **26**, 2623 (2009); S. Qiu and Y. P. Li, *ibid.* **26**, 1664 (2009).

[29] A. Taflove and S. C. Hagness, *Computational Electrodynamics: The Finite-Difference Time-Domain Method*, 2nd ed. (Artech House, Boston, MA, 2000).

[30] C. Lu, S. Chang, S. Chuang, T. Germann, and D. Bimberg, Appl. Phys. Lett. **96**, 251101 (2010); Z. Yu, G. Veronis, S. Fan, and M. Brongersma, *ibid.* **92**, 041117 (2008).

[31] See Supplemental Material at http://link.aps.org/supplemental/10.1103/PhysRevA.85.053803 for the multimedia file (movie) of the simulation corresponding to Fig. 7(e).